THE JOURNAL OF PHYSICAL CHEMISTRY A

A: Spectroscopy, Molecular Structure, and Quantum Chemistry

Complexes of Zn(II)-Triazoles with CO and HO: Structures, Energetics and Applications

Rahma Dahmani, Sonja Grubisic, Saida Ben Yaghlane, Salima Boughdiri, and Majdi Hochlaf

J. Phys. Chem. A, **Just Accepted Manuscript** • DOI: 10.1021/acs.jpca.9b03228 • Publication Date (Web): 04 Jun 2019

Just Accepted

is published by the American Chemical Society. 1155 Sixteenth Street N.W., Washington, DC 20036

Complexes of Zn(II)-triazoles with CO_2 and H_2O: Structures, Energetics and Applications

Rahma Dahmani,[a,b] Sonja Grubišić,[c,*] Saida Ben Yaghlane,[d] Salima Boughdiri,[b] and Majdi Hochlaf [a,*]

[a] Université Paris-Est, Laboratoire Modélisation et Simulation Multi Echelle, MSME UMR 8208 CNRS, 5 Bd Descartes, 77454 Marne- La-Vallée, France.

[b] Université Tunis El Manar, Faculté des Sciences de Tunis, Laboratoire de caractérisations, applications et modélisations des matériaux, 2092, Tunis, Tunisia.

[c] Center for Chemistry, ICTM, University of Belgrade, Njegoševa 12, P.O. Box 815, 11001 Belgrade, Serbia.

[d] Université Tunis El Manar, Faculté des Sciences de Tunis, Laboratoire de Spectroscopie Atomique, Moléculaire et Applications – LSAMA, 2092, Tunis, Tunisia.

* authors to whom correspondence should be addressed.

Emails: S. Grubišić: grubisic@chem.bg.ac.rs;

M. Hochlaf: hochlaf@univ-mlv.fr

Abstract

Using first principle methodology, we investigate the stable structures of the non-reactive and reactive clusters formed between Zn^{2+}-triazoles ([Zn^{2+}-Tz]) clusters and CO_2 and / or H_2O. In sum, we characterized two modes of bonding of [Zn^{2+}-Tz] with CO_2/H_2O: (i) The interaction is established through a covalent bond between Zn^{2+} of [Zn^{2+}-Tz] and oxygen atoms of CO_2 or H_2O; and (ii) hydrogen bonds through N–H or C–H of [Zn^{2+}-Tz] and oxygen atom of H_2O or CO_2, N–H---O. We also identified intramolecular proton transfer processes induced by complexation. Indeed, water changes drastically the shape of the energy profiles of the tautomeric phenomena, through a strong lowering of the potential barriers to tautomerism. The comparison to [Zn^{2+}-Im] subunits formed with Zn^{2+} and imidazole shows that the efficiency of Tz based compounds for CO_2 capture and uptake is due to the incorporation of more accessible nitrogen donor sites in Tzs compared to imidazoles. Since [Zn^{2+}-Tz] clusters are subunits of organometallic nanoporous material and Zn-proteins, our data are useful for deriving force fields for macromolecular simulations of these materials. Our work suggests also the consideration of traces of water to better model the CO_2 sequestration and reactivity on these macromolecular entities pores or active sites.

I. Introduction

Metal-triazole or metal-triazole derivatives, such as those formed between triazoles and Zn(II), Cd(II) and Hg(II) ions, [1] are subunits of macromolecular porous materials and metalloenzymes and of promising pharmacological compounds. They are linked to diverse applications of primary importance in biology, medicine, industry, environment and material science. In biology and medicine, 1,2,3-triazole@Zn^{2+} complexes are potentially used to mimic histidine-carboxylate active site of metallopeptidases, [2] which is connected with the catalytic conversion of CO_2 in biological media. [3 4 5 6 7 8 9] We can also find these entities in antibacterial drugs. Indeed, Amitrole (3-amino-1,2,4-triazole) is a widely used herbicide that inhibits an enzyme of histidine biosynthesis in Salmonella typhimurium. [10] Triazoles also have the highest potential for antifungal drugs. Indeed, they are confirmed as inhibitors of various hepatic CYP450 metabolic enzymes [11] and some of other triazole compounds, e.g., 3-substituted-4-amino-5-mercapto-1,2,4-triazoles, were found to be active against some cancer cells. [12] Moreover, these organometallic entities are the backbones of metal organic frameworks (MOFs), [13] polynuclear metal complexes, [14] hybrid coordination polymers, highly hydrophobic porous organic polymers, [15] 1D ring-like infinite chains polymers [16] functionalized fluorescent polymer nanospheres, [17] functionalized podand triazole-linked gold nanoparticles, [18] mixed metal metal-organic polyhedra networks, colloids, highly porous (3,24)-connected framework NTU-105, [19] and advanced electrodes.

Nanopourous materials with various structures and properties can be obtained via different combinations of metal centers and organic ligands. The coordination number of the metal and the geometry around the metal have vital roles for applications. [20 21] For instance, they are on the origin of the 3D structure of the pore cavity in nanoporous materials (e.g. MOFs), which is essential to their use for the selective and specific gas (e.g. H_2, CO_2) adsorption capture, sequestration. In addition, the adsorption capacity of MOFs depends on the choice of the organic linkers and metals. Recent studies revealed that organic linkers containing N-rich heterocycles, such as triazoles, are very efficient for CO_2 adsorption [22 23 24] The triazoles exceptional capacity and selectivity for gas adsorption is attributed to the relatively strong van der Waals interactions between CO_2 and amine functionalities. [25]

Numerous investigations showed that the presence of water might affect the adsorption of CO_2 on nanoporous materials. For instance, Joos et al. [26] showed that the presence of water reduces, by an order of magnitude, the adsorption capacity of CO_2 in zeolite 13X, which is the most common commercial adsorbent used for CO_2 capture. Li et al. [27 28] noticed also that the CO_2 purity using zeolite 13X decreases from 95% to 59% in dry air CO_2 (10-12 % of CO_2) and in wet CO_2 flue gas steams containing 3.4% (vol), respectively. However, Yazaydin et al. [29] proved, through experiments and simulations, the opposite effect.

According to their results, the introduction of 4 wt % water molecules increases the coulombic interactions between water molecules and CO_2, and thus favors the CO_2 uptake by 45% at 1 bar. These electrostatic interactions arise from the electric field generated by water molecules and quadrupole moment of CO_2. In addition, Soubeyrand-Lenoir et al. [30] reported a remarkable increase of CO_2 uptake in MIL-100(Fe) at low pressure (0.2 bar), whereas, further increasing of water loading may block the CO_2 uptake.

Recent works showed that the decrease of CO_2 uptake in the presence of water may be related to the change of the surface pores after their reaction with water, thus enhancing or decreasing locally their Brønsted acidity. [31] Generally, water stability in adsorbent depends on the steric effect around the ligand and coordination sites in materials [32]. Such laboratory observations are closely connected with the industrial and catalytic applications of metal-triazole or metal-triazole derivatives based macromolecular entities. Note that it is difficult to understand the phenomena occurring at the surface of the pores of these materials without simulations at the microscopic level. This is because the latters allow screening individual elementary processes of "ideal" systems, whereas experiments mostly probe integral or global information of "non-ideal" systems. The induced reactivity, binding and nano-confinement effects due to the introduction of ligands binding moieties in surface pores are still poorly understood.

Experimental and theoretical studies of the Zn-organic linker backbones interacting with water or CO_2 remain very limited. Theoretically, we can cite, for instance, our recent work on CO_2 interacting with Zn^{q+}–imidazole (q=0, 1, 2) complexes [33] or with imidazole attached on gold clusters and surface [34], that of Linder et al. [35] on $[(H_2O)@Zn–(imidazole)_n]^{2+}$ complexes, and of Grauffel and Lim [36] on $[(H_2O)@Zn–(AA)_n]^{2+}$ (AA: amino acid modeled by imidazole or methylimidazole) clusters. Experimentally, the review by Parkin [37] gives a detailed presentation on the synthesis and characterization of medium sized Zn(II) based motifs found in Zn enzymes. Other examples can be found in Ref. [38]. For instance, a description of the determination of the binding energy of $H_2O@Zn–(Im)_3^{2+}$ by Peschke et al. [39] is given there.

In a recent work we characterized the stable structures of the complexes formed between zinc II (Zn^{2+}) and 1H-1,2,3-triazole, 2H-1,2,3-triazole, 1H-1,2,4-triazole and 4H-1,2,4-triazole. [40] These clusters are denoted [Zn^{2+}-Tz] and displayed in Figure 1, where we follow the denomination as given in Ref. [34]. Briefly, we determined seven [Zn^{2+}-Tz] complexes in which the bounding is ensured by σ-type bond formed after in-plane favorable interactions between Zn^{2+} and the unprotonated nitrogen atom of triazole or via out-of-plane interactions between C_5 atom of Tz and Zn^{2+}. These forms serve as starting point for the studies $CO_2@[Zn^{2+}$-Tz], $H_2O@[Zn^{2+}$-Tz] and of $CO_2@H_2O@[Zn^{2+}$-Tz] clusters that we will

investigate herein. In this work, we identified their equilibrium structures, binding positions, binding energies, and relative stabilities in gas phase and in water solution. Although the metal ion (Zn^{2+}) is able to form stable complexes with more than one Tz ligand, we only investigated complexes with 1:1 stoichiometric ratio (i.e., 1 Zn (II) : 1 Tz) in order to study in more detail the interactions between H_2O/CO_2 and [Zn^{2+}-Tz] complexes at the molecular level. Mainly, we identified two major classes of complexes formed, which are: the weakly bound complexes, and the Zn-O covalently bonded complexes. For the former ones, the clustering occurs via van der Waals and H-bonding interactions between Tz and CO_2 and/or H_2O. For the complexes containing Zn-O bond, the CO_2 and/or H_2O reacts with the metallic center. For a tetra (or hexa)-coordination zinc will make the system larger and will be the subject of our future study.

The evaluation of solvent-solute interactions of CO_2@[Zn^{2+}-Tz] in the presence of water is important since water may affect the coordination sites and stability of [Zn^{2+}-Tz] and their complexes with CO_2. Thus, we identified the hydrophilic sites of [Zn^{2+}-Tz] complexes and the coordination sites between [Zn^{2+}-Tz] and CO_2 in the presence of one water molecule in gas phase. Also, we investigated the 1,2 proton transfer mechanism, in gas phase and in water solution, of two CO_2@[Zn^{2+}-Tz] tautomers. Afterwards, we will use our findings to discuss the tautomeric equilibrium in solution and to propose an explanation for the observed features in the macromolecular entities. The new predicted complex isomers may be used for the design of new materials since only the structures of dominant tautomers are known experimentally.

II. Computational details

Experimental bond lengths, binding energies and deprotonation energies are not available for Zn(II) complexes investigated in this study. According to Truhlar and co-workers [41] [42] the M05-2X DFT [43] performs very well to predict energetics and geometric properties of Zn(II) organo complexes. Moreover and through systematic studies of complexes formed between Zn^{2+} and nitrogen rich five member ring heterocycles [40] [44] [33], we highlighted the ability of M05-2X and PBE0 density functionals with dispersion correction (+D3 [45]) to accurately describe both covalent and weak interactions (H- bonds and van der Waals) between Zn^{2+} and triazoles (Tz). Indeed, a close agreement with the costly *ab initio* CCSD(T) and CCSD(T)-F12 results is observed, whereas the cost of the computations is strongly reduced when using DFT(+D3). [40] Therefore, the present theoretical study is performed using M05-2X(+D3) functional to investigate the structures, the stability, and the bonding of CO_2@[Zn^{2+}-Tz], H_2O@[Zn^{2+}-Tz] and CO_2@H_2O@[Zn^{2+}-Tz] complexes. These electronic structure computations were carried out using GAUSSIAN 09 (version D0.1)

package. [46] The choice of the basis set is based on previous reports dealing with metal–ligand complexes and CO_2 adsorption on Zn complexes. [33] These works tested the suitability of extended basis set (6-311++G**) to describe metal-organic compounds at a relatively small computational cost.

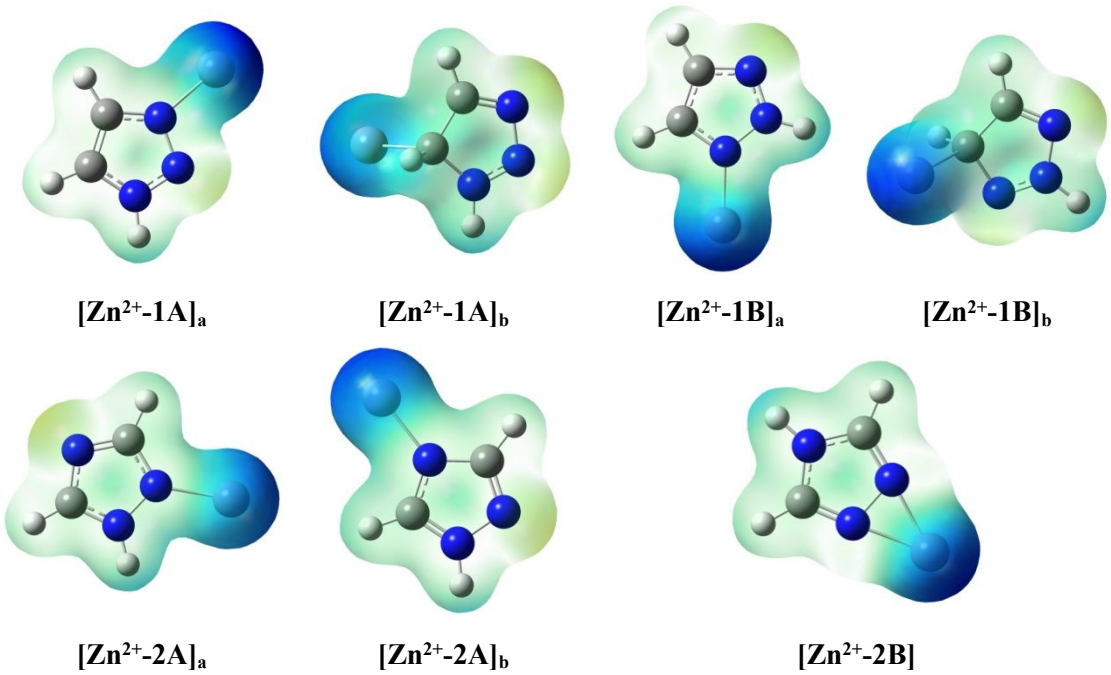

Figure 1: Equilibrium structures of [Zn^{2+}-Tz] complexes as determined in Ref. [40]. **1A** is for 1H-1,2,3-triazole, **1B** is for 2H-1,2,3-triazole, **2A** is for 1H-1,2,4-triazole and **2B** is for 4H-1,2,4-triazole. We give also the 3D electrostatic potential surface maps (3D MESP, isovalue 0.01 e/au^3) of [Zn^{2+}-Tz] complexes as computed using GAUSSIAN.

As a starting point, we considered the [Zn^{2+}-Tz] clusters as identified in Ref. [40] i.e. [Zn^{2+}-1A]$_a$, [Zn^{2+}-1A]$_b$, [Zn^{2+}-1B]$_a$, [Zn^{2+}-1B]$_b$, [Zn^{2+}-2A]$_a$, [Zn^{2+}-2A]$_b$ and [Zn^{2+}-2B]. They are displayed in Figure 1. There would be a diversity of clusters in interaction with CO_2 / H_2O. This complicates the present study since a large number of CO_2@[Zn^{2+}-Tz], of H_2O@[Zn^{2+}-Tz] and of CO_2@H_2O@[Zn^{2+}-Tz] complexes is expected. Firstly, a systematic search of the minimal structures formed by the [Zn^{2+}-Tz] clusters with CO_2 and/or H_2O in gas phase at the M05-2X+D3/6-311++G** level of theory has been performed. Then we carried out polarizable continuum method (PCM, solvent=water) [47] [48] simulations of the resulting CO_2@[Zn^{2+}-Tz] complexes at the same level of theory to account for implicit solvation effects on the coordination site, the bonding, and stability of these systems. Secondly, we computed the intracluster 1,2 proton transfer mechanism, in gas phase and in water solution, of two potential tautomers.

We fully optimized the geometries without symmetry constraints, in the C_1 point group. In each step of theoretical study, we have confirmed by vibrational analysis that all equilibrium structures (true minima) correspond to stationary points on the potential energy surfaces without any imaginary frequency. For transition states, we computed stationary points with one imaginary frequency. For each transition state existing on the potential energy surface, intrinsic reaction coordinate (IRC) [49] [50] calculations were performed to ascertain that it connects the desired species. We followed reaction path in both directions (forward path: from TS to products and reverse path: from TS to reactants).

In order to evaluate the inter / intra molecular charge transfer within the complexes, we carried out Natural Bond Orbital analysis NBO6 [51] at the M05-2X+D3/6-311++G** level of theory under Gaussian program package. Most of the details and results are given in the Supplementary Information. We further characterized these complexes by computing their binding energies (BEs). These calculations help evaluating their strength and stability. As the use of finite basis set in quantum chemical calculations leads to basis set superposition error (BSSE), i.e. either lowering energy of the dimer or unrealistic large stabilization, BEs were corrected for BSSE using the counterpoise procedure as suggested by Boys and Bernardi [52] and expressed as follows:

$$BE = E_{AB} - (E_A + E_B)$$

where BE is the binding energy of complex AB at equilibrium; E_{AB} is the total energy of AB at equilibrium; E_A is the energy of A at equilibrium; E_B is the energy of B at equilibrium. These three terms are evaluated in the AB complex basis set. For CO_2@[Zn^{2+}-Tz] and CO_2@H_2O@[Zn^{2+}-Tz], B is CO_2 and for H_2O@[Zn^{2+}-Tz], B is H_2O.

III. Results : Bonding and equilibrium structures

Figure 1 presents the equilibrium structures of [Zn^{2+}-Tz] clusters as determined in Ref. [40]. These structures served as starting point to bind CO_2, H_2O or both. We also give in Figure 1 the 3D electrostatic potential surface maps (3D MESP) of [Zn^{2+}-Tz] species. These 3D MESP correspond to the electrostatic potential of [Zn^{2+}-Tz] complexes due to their electron charge densities extending around them. Their examination allows assessing the possible binding sites of these complexes using simple electrostatic considerations. Indeed, this figure shows that, as expected, the Zn atom exhibits a strong positive potential. Thus, it will be subject to nucleophilic attacks by O atoms of CO_2 and of H_2O. Whereas Tzs may be involved in nucleophilic attacks at the H bonded to N or C by the O of CO_2 and H_2O, or electrophilic attacks at the N lone pairs either by the C of CO_2 or by the H of H_2O. The optimized stable CO_2@[Zn^{2+}-Tz], H_2O@[Zn^{2+}-Tz] and CO_2@H_2O@[Zn^{2+}-Tz] complexes are depicted in Figures 2, 3 and 4, respectively. All these structures correspond to minima in the

corresponding potential energy surface. The complexes between [Zn^{2+}-Tz] and H_2O or CO_2 are denoted as $YY@XX_{,Si}$ where XX stands for the [Zn^{2+}-Tz] cluster used (cf. Figure 1), YY is for CO_2 or H_2O and "Si" (i = 1, 2, …) is the numbering of the complexes for their classification. For complexes involving CO_2 and H_2O and [Zn^{2+}-Tz] we use the $CO_2@H_2O@XX_{,Si}$ notation. We give their coordinates in the Supplementary Information.

a. CO_2@[Zn^{2+}-Tz] complexes

Table 1: Intermonomer distances (in Å) of CO_2@[Zn^{2+}-Tz] complexes and their binding energies (BE, in kcal.mol^{-1}) in gas phase and in water solution as computed at the M05-2X+D3/-311++G** level of theory. See Figure 2 for the denomination of the clusters and for the definition of the quoted distances.

	Gas Phase			PCM Solvent model	
	Distances		BE	Distances	BE
$CO_2@[Zn^{2+}\text{-}1A]_{b,S1}$	R_1 R_2	2.505 2.768	-12.02	3.054 3.134	-7.61
$CO_2@[Zn^{2+}\text{-}1A]_{a,S2}$	R	1.881	-56.42	2.099	-48.04
$CO_2@[Zn^{2+}\text{-}1A]_{a,S3}$	R_1 R_2	2.447 2.523	-7.94	2.693 2.661	-6.70
$CO_2@[Zn^{2+}\text{-}1A]_{a,S4}$	R	1.761	-12.04	2.078	-9.00
$CO_2@[Zn^{2+}\text{-}1B]_{b,S1}$	R	1.897	-52.79	2.144	-43.23
$CO_2@[Zn^{2+}\text{-}1B]_{b,S2}$	R	1.666	-14.32	2.069	-9.98
$CO_2@[Zn^{2+}\text{-}1B]_{a,S3}$	R	1.878	-58.58	2.136	-47.74
$CO_2@[Zn^{2+}\text{-}1B]_{a,S4}$	R_1 R_2	2.309 2.686	-8.16	2.332 2.761	-6.64
$CO_2@[Zn^{2+}\text{-}2A]_{a,S1}$	R	1.880	-57.73	2.136	-46.86
$CO_2@[Zn^{2+}\text{-}2A]_{b,S2}$	R	1.882	-56.83	2.129	-47.85
$CO_2@[Zn^{2+}\text{-}2A]_{b,S3}$	R	1.756	-11.91	2.053	-9.74
$CO_2@[Zn^{2+}\text{-}2B]_{S1}$	R	1.899	-51.74	2.139 [a)]	-45.15
$CO_2@[Zn^{2+}\text{-}2B]_{S2}$	R	1.750	-12.85	2.103 [a)]	-9.71

a. With PCM solvation, the zinc ion is no more bonded to triazole through two nitrogens (CO_2@[Zn^{2+}-2B]) but through only one covalent bond.

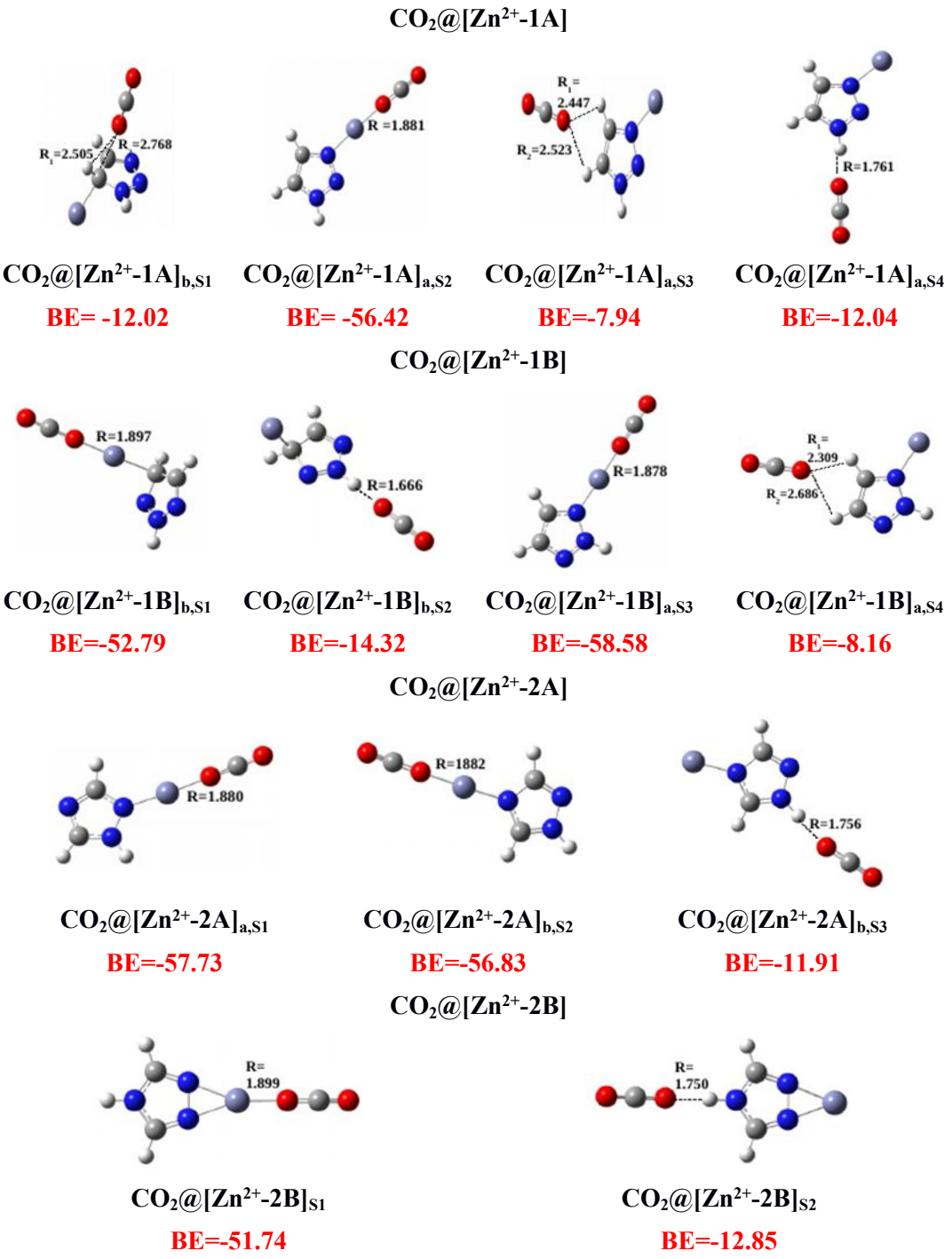

Figure 2: M05-2X+D3/-311++G** optimized equilibrium structures between CO_2 and [Zn^{2+}-Tz] complexes. We give also their intermonomer distances and their gas phase binding energies (BE, in kcal.mol^{-1}).

We mapped the ground state potential energy surface (PES) of CO_2@[Zn^{2+}-Tz] to locate the possible coordination sites between [Zn^{2+}-Tz] (Figure 1) and CO_2, where a systematic search of all possible positions of CO_2 around [Zn^{2+}-Tz] was carried out. We give in Figure 2 the equilibrium structures of CO_2 interacting with [Zn^{2+}-Tz] complexes which are

identified using the M05-2X+D3 functional in conjunction with the 6-311++G** basis set.

For CO_2 interacting with [Zn^{2+}-1A], four forms were obtained where CO_2 binds to 1A Tz in CO_2@[Zn^{2+}-1A]$_{b,S1}$, CO_2@[Zn^{2+}-1A]$_{a,S3}$ and CO_2@[Zn^{2+}-1A]$_{a,S4}$ and where CO_2 is linked to zinc in CO_2@[Zn^{2+}-1A]$_{a,S2}$. For CO_2@[Zn^{2+}-1B], two clusters (CO_2@[Zn^{2+}-1B]$_{b,S1}$ and CO_2@[Zn^{2+}-1B]$_{a,S3}$) were found where CO_2 interacts directly with zinc. For CO_2@[Zn^{2+}-2A], we compute a weakly bond complex where CO_2 interacts with 2A Tz and two clusters (CO_2@[Zn^{2+}-2A]$_{a,S1}$ and CO_2@[Zn^{2+}-2A]$_{b,S2}$) where CO_2 is attached to zinc. When CO_2 is approaching [Zn^{2+}-2B], two isomers are formed: CO_2 is linked either to zinc (CO_2@[Zn^{2+}-2B]$_{S1}$) or to 2B Tz (CO_2@[Zn^{2+}-2B]$_{S2}$). All clusters are planar except CO_2@[Zn^{2+}-1A]$_{b,S1}$, CO_2@[Zn^{2+}-1B]$_{b,S1}$ and CO_2@[Zn^{2+}-1B]$_{b,S2}$. Note that the majority of the structures in gas phase have similar complexes in water solution (see Table 1 for more details).

Figure 2 and Table 1 present the intermonomer distances between the oxygen atom of CO_2 and the coordination site of [Zn^{2+}-Tz] complexes and their binding energies BEs as computed at the M05-2X+D3/6-311++G** level of theory in gas phase and in water solution. This table shows that the CO_2 -- [Zn^{2+}-Tz] distances are longer in the solvent whereas the BEs are lowered by several kcal/mol. Moreover, Table 1 shows that the most stable structures are strong electron donor-acceptor complexes, in which a covalent Zn–O bond between CO_2 and Zn^{2+} is established: CO_2@[Zn^{2+}-1A]$_{a,S2}$, CO_2@[Zn^{2+}-1B]$_{b,S1}$, CO_2@[Zn^{2+}-1B]$_{a,S3}$, CO_2@[Zn^{2+}-2A]$_{a,S1}$, CO_2@[Zn^{2+}-2A]$_{b,S2}$ and CO_2@[Zn^{2+}-2B]$_{S1}$ with Zn–O distances amounting to 1.881, 1.897, 1.878, 1.880, 1.882, and 1.899 (in Å), respectively. The order of stability of theses complexes, in the gas phase, is CO_2@[Zn^{2+}-1B]$_{a,S3}$ > CO_2@[Zn^{2+}-2A]$_{a,S1}$ > CO_2@[Zn^{2+}-2A]$_{b,S2}$ > CO_2@[Zn^{2+}-1A]$_{a,S2}$ > CO_2@[Zn^{2+}-1B]$_{b,S1}$ > CO_2@[Zn^{2+}-2B]$_{S1}$ for which we compute the following M05-2X+D3/6-311++G** BEs (in kcal/mol) -58.58, -57.73, -56.83, -56.42, -52.79 and -51.74, respectively. In PCM water solvent model, these BEs are in the range of -48 to -43 kcal/mol and their ordering in energy is slightly changed. Such BE reduction upon solvation is expected since in water solution the Zn–O bond is longer and thus weaker. They represent models, at the microscopic level, of the interaction of CO_2 with Zn of Zn-enzymes at their active sites.

Second order perturbation energy (E_2) and NBO analysis as given in the Supplementary Information, show that the Zn–O containing complexes are due to interaction through coordination bond between zinc of Tz and oxygen atom of CO_2. Thus, CO_2 forms a bond with Zn within these complexes. This is associated with intramolecular charge transfer within CO_2 from the lone pair (LP) of O to the C-O 2-center antibond (BD*) (E_2 > 90 kcal.mol^{-1}). Further stabilization of these complexes is due to intermonomer charge transfer from Tz to Zn (from LP(1) N →LV(1) Zn) and from CO_2 to Zn (from LP (1) O →LV(1) Zn).

The other clusters depicted in Figure 2 are formed by van der Waals type of

interactions between CO_2 and the organic part of [Zn^{2+}-Tz] via σ-type H-bonds. These H-bonds are of two types: (i) interaction through N–H---O with BEs ranging from -11.9 (CO_2@[Zn^{2+}-2A]$_{b,S3}$) to -14.32 (CO_2@[Zn^{2+}-1B]$_{b,S2}$) kcal/mol and (ii) C–H---O interactions with BEs much smaller (of ~ -8 kcal/mol). This type of interaction was only identified in 1,2,3-triazole (isomer 1A and isomer 1B) since the double bond is localized between the two carbon atoms of these isomers which is not the case for 1,2,4-triazole. See Supplementary Information for in depth analysis of their bonding.

For σ H-bond (through N-H—O) noncovalently interacting complexes, we identified an intermolecular charge transfer from the LP of O to the N-H BD*. These interactions are weak. As expected, we computed relatively small E_2 values of 17.52, 26.42, 17.50 and 18.72 kcal.mol^{-1} for CO_2@[Zn^{2+}-1A]$_{a,S4}$, CO_2@[Zn^{2+}-1B]$_{b,S2}$, CO_2@[Zn^{2+}-2A]$_{b,S3}$ and CO_2@[Zn^{2+}-2B]$_{S2}$, respectively. However, the stability of these complexes is ensured through intramolecular charge transfer within CO_2 (E_2 > 110 kcal.mol^{-1}). For the π-stacking type of noncovalent interaction in CO_2@[Zn^{2+}-1A]$_{a,S3}$ and CO_2@[Zn^{2+}-1B]$_{a,S4}$, we identified a charge transfer from LP of O to C-H BD* with very low E_2 (< 1 kcal.mol^{-1}). Again, we observe intramolecular charge transfer within CO_2 (E_2 > 133 kcal.mol^{-1}).

b. H_2O@[Zn^{2+}-Tz] complexes

We mapped the ground state potential energy surface (PES) of H_2O@[Zn^{2+}-Tz] to locate the possible coordination sites between [Zn^{2+}-Tz] and H_2O, to investigate their types of interactions and to identify the hydrophilic centers of [Zn^{2+}-Tz] complexes. Figure 3 presents the M05-2X+D3/6-311++G** equilibrium structures of H_2O@[Zn^{2+}-Tz] complexes, their binding energies and H_2O -- [Zn^{2+}-Tz] intermonomer distances. In total, 16 complexes are found between H_2O and [Zn^{2+}-Tz]. All of them exhibit an interaction between the O atom of H_2O and the [Zn^{2+}-Tz] moiety. As for CO_2@[Zn^{2+}-Tz], there are either clusters where H_2O is linked to Zn^{2+} or where H_2O is bonded via σ-type H-bonds. See Figure 3 for more details.

According to the values of BEs listed in Figure 3, the most stable monohydrated complexes have a Zn-O bond, which results from a covalent bonding between the unsaturated zinc metal ion of [Zn^{2+}-Tz] and the oxygen atom of H_2O. Within these complexes, the Zn-O distance amounts to ~1.9 Å. The order of stability of these complexes in gas phase is H_2O@[Zn^{2+}-1B]$_{a,S4}$, H_2O@[Zn^{2+}-2A]$_{a,S1}$, H_2O@[Zn^{2+}-2A]$_{b,S3}$, H_2O@[Zn^{2+}-1A]$_{a,S5}$, H_2O@[Zn^{2+}-1A]$_{a,S4}$, H_2O@[Zn^{2+}-1B]$_{b,S1}$, H_2O@[Zn^{2+}-2B]$_{S1}$, for which we compute the following BEs (in kcal/mol) -80.77, -79.93, -78.94, -78.58, -78.48, -74.36, and -74.22, respectively. In absolute value, these BEs are distinctly larger (by > 20 kcal/mol) than those computed for CO_2@[Zn^{2+}-Tz]. The second class of complexes feature weak interactions where H-bonds are formed either through N–H---O as in H_2O@[Zn^{2+}-1A]$_{a,S3}$ or H_2O@[Zn^{2+}-

1A]$_{a,S2}$; or through C–H---O as in $H_2O@[Zn^{2+}\text{-}1A]_{a,S6}$ or $H_2O@[Zn^{2+}\text{-}2A]_{a,S2}$. Note that the BEs of the latter complexes are smaller than the previous ones, but remain relatively large (in the range 40-17 kcal/mol, Figure 3), as signature of the large stability of water complexes with Zn-triazoles. This is accompanied by the shortening of the distances between H_2O and Tz.

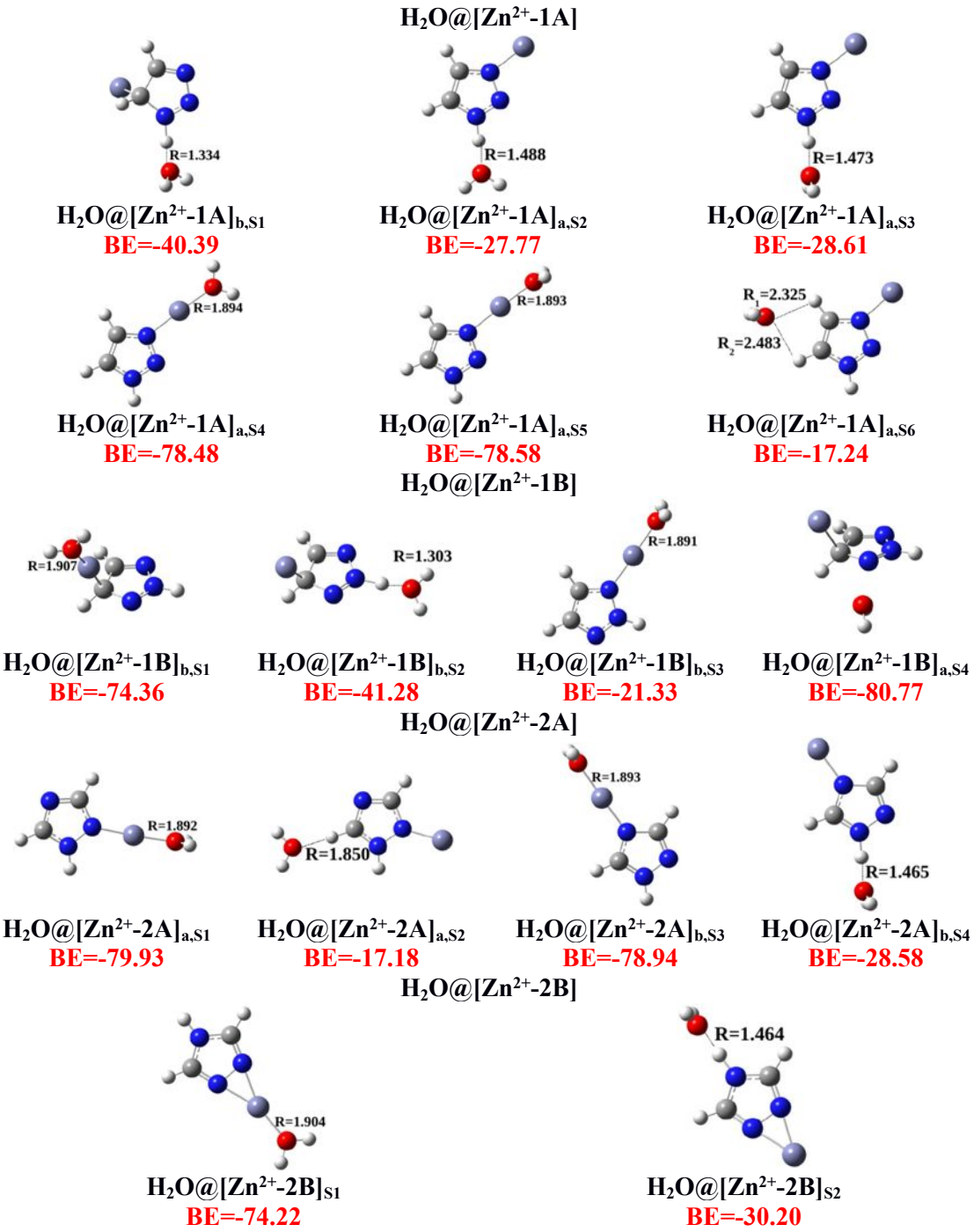

Figure 3: M05-2X+D3/-311++G** equilibrium structures of **$H_2O@[Zn^{2+}\text{-}Tz]$** complexes. We give also their intermonomer distances (in Å) and their binding energies (BE, in kcal.mol^{-1}) in gas phase.

We give, in the Supplementary Information, the analysis of the types of interaction, as are evidenced from second-order perturbation energy (E_2) values and NBO analysis. These data show the presence of three types of interactions between H_2O and [Zn^{2+}-Tz] complexes. The first one is a σ H-bond (through N-H—O) interaction, e.g., $H_2O@[Zn^{2+}\text{-}1A]_{b,S1}$, $H_2O@[Zn^{2+}\text{-}1A]_{a,S2}$, $H_2O@[Zn^{2+}\text{-}1A]_{a,S3}$, $H_2O@[Zn^{2+}\text{-}1B]_{b,S2}$, $H_2O@[Zn^{2+}\text{-}2A]_{b,S4}$ and $H_2O@[Zn^{2+}\text{-}2B]_{S2}$. These complexes are dominated by intermolecular charge transfer from the LP of the oxygen atom of H_2O to the N-H BD* of [Zn^{2+}-Tz]. Their E_2 values are given as follows, 119.08, 64.61, 67.96, 132.07, 71.43 and 70.40 kcal.mol^{-1}. For the complex with the highest E_2 value, $H_2O@[Zn^{2+}\text{-}1B]_{b,S2}$, we noted that the H_2O is in the same plane as Tz which favors the charge transfer. The second type of interaction is a π-stacking type (e.g. $H_2O@[Zn^{2+}\text{-}1A]_{a,S6}$). This complex is dominated by an intra molecular charge transfer within Tz (isomer 1A) from nitrogen LP to N–N BD* with E_2 equals to 105.65 kcal.mol^{-1}. Furthermore we identified a very weak charge transfer from the oxygen LP of H_2O to C-H BD* of Tz with very low E_2 value (< 1 kcal.mol^{-1}). The third type of interaction is associated with intermolecular charge transfer from oxygen LP of H_2O to Zn LV through coordination bond between O atom of H_2O and Zn in e.g. $H_2O@[Zn^{2+}\text{-}1A]_{a,S4}$, $H_2O@[Zn^{2+}\text{-}1A]_{a,S5}$, $H_2O@[Zn^{2+}\text{-}2A]_{a,S1}$ and $H_2O@[Zn^{2+}\text{-}2B]_{S1}$ with E_2 = 51.61, 51.80, 53.24 and 47.71 kcal.mol^{-1}, respectively. The stability of these complexes is ensured through intramolecular charge transfer within the Tz part of the complexes.

c. [Zn^{2+}-Tz] interacting with H_2O and CO_2

We used the stable monohydrated [Zn^{2+}-Tz] complexes as starting point, where a systematic search of all possible binding positions of CO_2 was performed. The CO_2 was turned around the $H_2O@[Zn^{2+}\text{-Tz}]$ trimer and let free to converge to the stable positions. Figure 4 shows the 25 equilibrium structures of the $CO_2@H_2O@[Zn^{2+}\text{-Tz}]$ complexes as computed at the M05-2X+D3/ 6-311++G** level of theory. They correspond to CO_2 or H_2O linked to Zn^{2+} or Tz part of the molecule and in few cases to CO_2 and H_2O interacting mutually with Zn^{2+} or Tz. This figure lists also their BSSE corrected BEs computed as the difference between the energies of CO_2 and $H_2O@[Zn^{2+}\text{-Tz}]$ entities. Mostly, these clusters can be viewed as CO_2 added to the $H_2O@[Zn^{2+}\text{-Tz}]$ complexes, without altering the later part. For instance, we list in Table 2 the matching between both sets of clusters.

Figure 3 shows that BEs for attaching CO_2 to $H_2O@[Zn^{2+}\text{-Tz}]$ are close to those computed above for $CO_2@[Zn^{2+}\text{-Tz}]$. The effect of H_2O can be viewed as a reduction of the BEs of CO_2 with [Zn^{2+}-Tz]. Indeed, Table 2 shows that the differences between the BEs of $CO_2@H_2O@[Zn^{2+}\text{-Tz}]$ and of $CO_2@[Zn^{2+}\text{-Tz}]$ are less than 3 kcal/mol, except for $CO_2@[Zn^{2+}\text{-}1B]_{a,S3}$ in which the BE value is increased by 20.13 kcal/mol. For the latter, this

is expected since the best hydrophilic site of $[Zn^{2+}\text{-}1B]_a$ corresponds to H_2O linked to zinc via covalent bond (i.e. $CO_2@H_2O@[Zn^{2+}\text{-}1B]_{a,S4}$ and $CO_2@H_2O@[Zn^{2+}\text{-}1B]_{a,S5}$).

Table 2: Matching between $CO_2@[Zn^{2+}\text{-Tz}]$ and $CO_2@H_2O@[Zn^{2+}\text{-Tz}]$ complexes. We give also $\Delta BE = |\mathbf{BE_{CO2@[Zn2+-Tz]}\text{-}BE_{CO2@H2O@[Zn2+-Tz]}}|$ (in kcal.mol^{-1}), which is the BE difference between the respective complexes.

$CO_2@[Zn^{2+}\text{-Tz}]$	$CO_2@H_2O@[Zn^{2+}\text{-Tz}]$	ΔBE
$CO_2@[Zn^{2+}\text{-}1A]_{b,S1}$	No match found	----
$CO_2@[Zn^{2+}\text{-}1A]_{a,S2}$	$CO_2@H_2O@[Zn^{2+}\text{-}1A]_{a,S2}$	2.39
$CO_2@[Zn^{2+}\text{-}1A]_{a,S3}$	$CO_2@H_2O@[Zn^{2+}\text{-}1A]_{a,S4}$	0.97
	$CO_2@H_2O@[Zn^{2+}\text{-}1A]_{a,S5}$	1.06
$CO_2@[Zn^{2+}\text{-}1A]_{a,S4}$	$CO_2@H_2O@[Zn^{2+}\text{-}1A]_{a,S6}$	1.36
	$CO_2@H_2O@[Zn^{2+}\text{-}1A]_{a,S7}$	0.96
$CO_2@[Zn^{2+}\text{-}1B]_{b,S1}$	$CO_2@H_2O@[Zn^{2+}\text{-}1B]_{b,S1}$	4.28
	$CO_2@H_2O@[Zn^{2+}\text{-}1B]_{b,S2}$	3.1
$CO_2@[Zn^{2+}\text{-}1B]_{b,S2}$	$CO_2@H_2O@[Zn^{2+}\text{-}1B]_{b,S3}$	1.4
$CO_2@[Zn^{2+}\text{-}1B]_{a,S3}$	$CO_2@H_2O@[Zn^{2+}\text{-}1B]_{a,S4}$	20.13
	$CO_2@H_2O@[Zn^{2+}\text{-}1B]_{a,S5}$	20.14
$CO_2@[Zn^{2+}\text{-}1B]_{a,S4}$	$CO_2@H_2O@[Zn^{2+}\text{-}1B]_{a,S6}$	1.05
$CO_2@[Zn^{2+}\text{-}2A]_{a,S1}$	$CO_2@H_2O@[Zn^{2+}\text{-}2A]_{a,S1}$	1.66
$CO_2@[Zn^{2+}\text{-}2A]_{b,S2}$	$CO_2@H_2O@[Zn^{2+}\text{-}2A]_{b,S6}$	2.46
$CO_2@[Zn^{2+}\text{-}2A]_{b,S3}$	$CO_2@H_2O@[Zn^{2+}\text{-}2A]_{b,S7}$	1.36
$CO_2@[Zn^{2+}\text{-}2B]_{S1}$	$CO_2@H_2O@[Zn^{2+}\text{-}2B]_{S1}$	2.54
$CO_2@[Zn^{2+}\text{-}2B]_{S2}$	$CO_2@H_2O@[Zn^{2+}\text{-}2B]_{S4}$	1.46

$CO_2@H_2O@[Zn^{2+}\text{-}1A]$

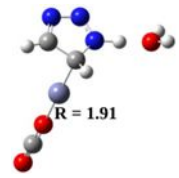

$CO_2@H_2O@[Zn^{2+}\text{-}1A]_{b,S1}$

BE = -49.23

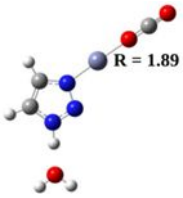

$CO_2@H_2O@[Zn^{2+}\text{-}1A]_{a,S2}$

BE = -54.03

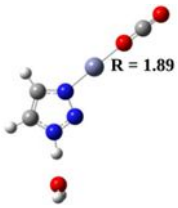

$CO_2@H_2O@[Zn^{2+}\text{-}1A]_{a,S3}$

BE = -53.96

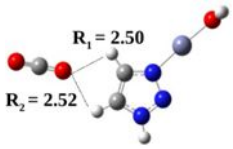

$CO_2@H_2O@[Zn^{2+}\text{-}1A]_{a,S4}$

BE = -6.97

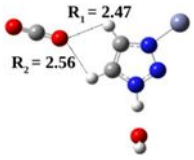

$CO_2@H_2O@[Zn^{2+}\text{-}1A]_{a,S5}$

BE = -6.88

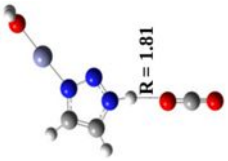

$CO_2@H_2O@[Zn^{2+}\text{-}1A]_{a,S6}$

BE = -10.68

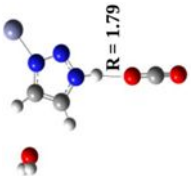

$CO_2@H_2O@[Zn^{2+}\text{-}1A]_{a,S7}$

BE = -11.08

$CO_2@H_2O@[Zn^{2+}\text{-}1B]$

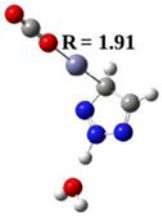

$CO_2@H_2O@[Zn^{2+}\text{-}1B]_{b,S1}$

BE = -48.51

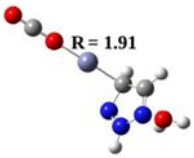

$CO_2@H_2O@[Zn^{2+}\text{-}1B]_{b,S2}$

BE = -49.69

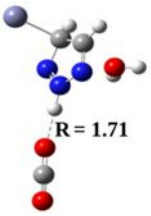

$CO_2@H_2O@[Zn^{2+}\text{-}1B]_{b,S3}$

BE = -12.92

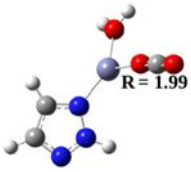

$CO_2@H_2O@[Zn^{2+}\text{-}1B]_{a,S4}$

BE = -38.45

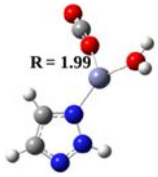

$CO_2@H_2O@[Zn^{2+}\text{-}1B]_{a,S5}$

BE = -38.44

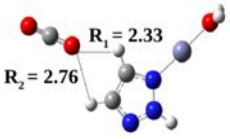

$CO_2@H_2O@[Zn^{2+}\text{-}1B]_{a,S6}$

BE = -7.11

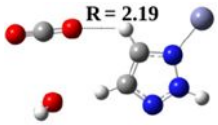

$CO_2@H_2O@[Zn^{2+}\text{-}1B]_{a,S7}$

BE = -8.85

$CO_2@H_2O@[Zn^{2+}\text{-}2A]$

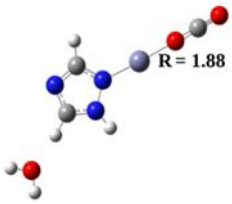

$CO_2@H_2O@[Zn^{2+}\text{-}2A]_{a,S1}$

BE = -56.07

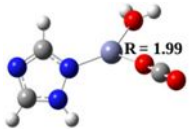

$CO_2@H_2O@[Zn^{2+}\text{-}2A]_{a,S2}$

BE = -37.76

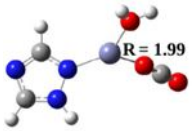

$CO_2@H_2O@[Zn^{2+}\text{-}2A]_{a,S3}$

BE = -37.76

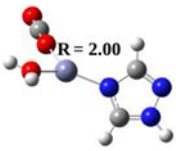

$CO_2@H_2O@[Zn^{2+}\text{-}2A]_{b,S4}$

BE = -36.45

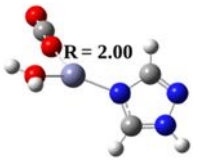

$CO_2@H_2O@[Zn^{2+}\text{-}2A]_{b,S5}$

BE = -36.56

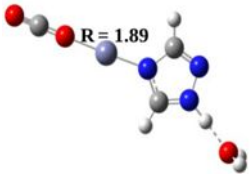

$CO_2@H_2O@[Zn^{2+}\text{-}2A]_{b,S6}$

BE = -54.37

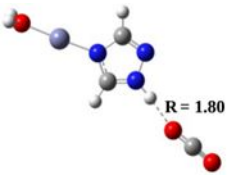

$CO_2@H_2O@[Zn^{2+}\text{-}2A]_{b,S7}$

BE = -10.55

$CO_2@H_2O@[Zn^{2+}\text{-}2B]$

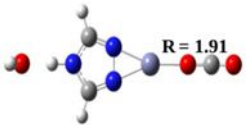

$CO_2@H_2O@[Zn^{2+}\text{-}2B]_{S1}$

BE = -49.20

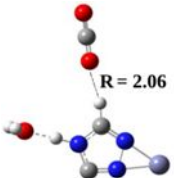

$CO_2@H_2O@[Zn^{2+}\text{-}2B]_{S2}$

BE = -7.10

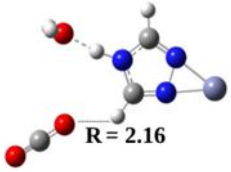

$CO_2@H_2O@[Zn^{2+}\text{-}2B]_{S3}$

BE = -7.18

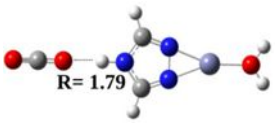

$CO_2@H_2O@[Zn^{2+}\text{-}2B]_{S4}$

BE = -11.39

Figure 4: M05-2X+D3/-311++G** equilibrium structures of $CO_2@H_2O@[Zn^{2+}$-Tz] complexes. We give also their intermonomer distances (in Å) and their binding energies (BE, in kcal.mol^{-1}) in gas phase.

We performed an NBO analysis to identify the most important interactions, responsible for the stability of the identified complexes. We list in Table S3 of the Supplementary Information (SI) the most important inter- and intra- molecular charge transfer identified for these complexes. Mostly, we identified the same type of interactions with and without the presence of H_2O: two non-covalently interacting complexes as σ H-bond (through N-H—O) and π-stacking and one covalent interaction through coordination bond between zinc attached to Tz and the oxygen atom of CO_2. All complexes are dominated by intramolecular charge transfer within CO_2 (with E_2 > 90 kcal.mol^{-1}). Further stabilization of these complexes is due to inter monomer charge transfer for each type of interaction. As for the complexes with covalent bond (such as $CO_2@H_2O@[Zn^{2+}$-1A$]_{a,S3}$ and $CO_2@H_2O@[Zn^{2+}$-2A$]_{a,S1}$), the intermolecular charge transfer is established from the oxygen LP to zinc LV (E_2 ~ 42 kcal.mol^{-1}). For σ H-bond, we identified an intermolecular charge transfer from oxygen LP of CO_2 to N-H BD* of Tz. These interactions are relatively weak. For example the E_2 value of $CO_2@H_2O@[Zn^{2+}$-2B$]_{S4}$ complex is ~ 15 kcal.mol^{-1}. For the π-stacking complexes, the intermolecular charge transfer from CO_2 to Tz is very weak and the dominant one is from H_2O to Tz (e.g. $CO_2@H_2O@[Zn^{2+}$-1A$]_{a,S4}$ and $CO_2@H_2O@[Zn^{2+}$-1A$]_{a,S5}$) with E_2 values of 51.76 and 60.01 kcal.mol^{-1} , respectively.

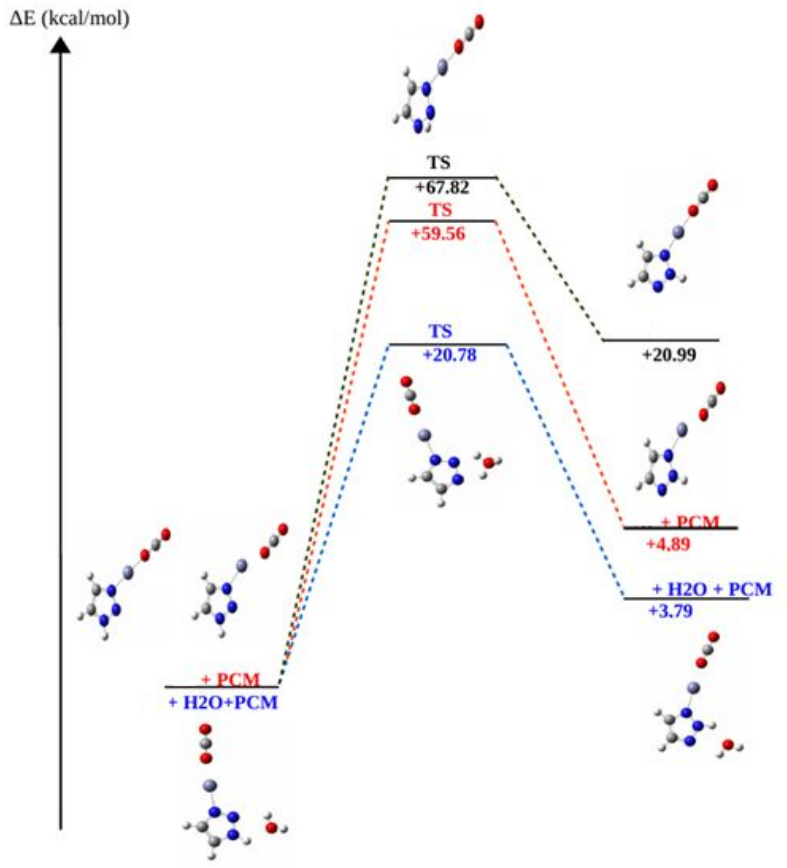

Figure 5: M05-2X+D3/6-311++G** potential energy profiles for the tautomerization reaction pathway of $CO_2@[Zn^{2+}\text{-}1A]_{a,S2}$ (left) – $CO_2@[Zn^{2+}\text{-}1B]_{a,S3}$ (right) in gas phase (black lines) and water solution with (blue lines) and without (red lines) the presence of an explicit water molecule. The reference energy is the energy of the initial reactants.

For triazoles, Cox et al. [53] indicated that the 2H tautomer (2H-1,2,3-triazole) is the only species observed in the gas phase, whereas both 2H and 1H tautomers (1H-1,2,3-triazole) are often observed in solution. Therefore, water, either explicitly and/or implicitly should influence the relative stability of the clusters we computed and their intramolecular tautomerisation. For illustration, we show in Figure 5 the mechanism of tautomerization between $CO_2@[Zn^{2+}\text{-}1A]_{a,S2}$ and $CO_2@[Zn^{2+}\text{-}1B]_{a,S3}$ in gas phase, and in water solution with and without the presence of a water molecule. In gas phase, $CO_2@[Zn^{2+}\text{-}1A]_{a,S2}$ is distinctly more stable than $CO_2@[Zn^{2+}\text{-}1B]_{a,S3}$, whereas in water environment both $CO_2@[Zn^{2+}\text{-}1A]_{a,S2}$ and $CO_2@[Zn^{2+}\text{-}1B]_{a,S3}$ tautomers possess close relative energies (energy difference is very small, ~ 4.89 kcal/mol). Thus, we expect to have dominantly $CO_2@[Zn^{2+}\text{-}1A]_{a,S2}$ in gas phase, whereas both $CO_2@[Zn^{2+}\text{-}1A]_{a,S2}$ and $CO_2@[Zn^{2+}\text{-}1B]_{a,S3}$ species should be present in aqueous solutions. Figure 5 shows however that both forms are separated by large potential barriers, which amount to 67.82 kcal/mol in gas phase, reduced to 59.56 kcal/mol in PCM

water solvent and, more interestingly, to 20.78 kcal/mol in the presence of an explicit water molecule. Thus, the presence of one water molecule decreases the activation barrier of proton transfer by a large amount of energy, facilitating the proton migration from nitrogen 1 to nitrogen 2 as discussed in Ref. [54] [55]. The covalent bond between zinc ion and nitrogen atom spreads the electronic charge from nitrogen atoms engaged in proton transfer into the rest of triazole ring. The bonding between nitrogen atoms and the hydrogen becomes weaker and the distance between hydrogen and water become smaller. However, the proton migrates first from triazole of CO_2@[Zn^{2+}-1A]$_{a,S2}$ to water, forming an anion-like TS, and finally from water to triazole to form CO_2@[Zn^{2+}-1B]$_{a,S3}$. Despite the decrease of activation energy of 1,2 proton transfer in water solution, there is still a relatively high energy barrier to overcome, which could be explained by the simultaneous transfer of two protons.

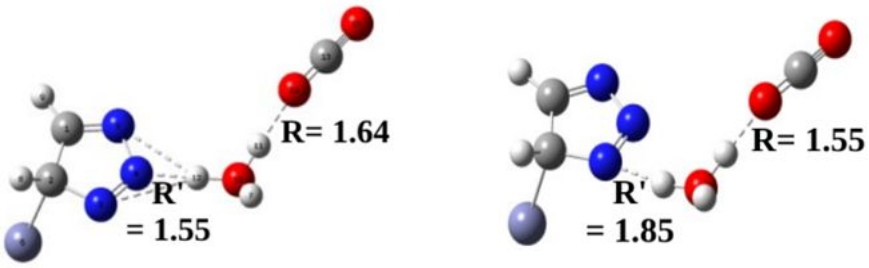

ΔE_{inter} = -13.60 ΔE_{inter} = -16.34

S1 **S2**

Figure 6: M05-2X+D3/-311++G** equilibrium structures of reactive compounds of CO_2@H_2O@[Zn^{2+}-Tz]. We give also their intermonomer distances (in Å) and their interaction energies (ΔE_{inter}, in kcal.mol^{-1}) as computed at the M05-2X+D3/-311++G** level of theory. For S1, ΔE_{inter} = E(S1) - (E(H_2O@[Zn^{2+}-Tz]) + E(CO_2)), where E stands for the total energy of the corresponding species. For S2, ΔE_{inter} = E(S2) - (E(H_2O@[Zn^{2+}-Tz]) + E(CO_2)), where E stands for the total energy of the corresponding species.

In addition to the van der Waals complexes discussed above, we observed proton transfer between H_2O and [Zn^{2+}-Tz] in the presence of CO_2. These reactive complexes are presented in Figure 6. Indeed, the presence of H_2O disturbs the interaction between CO_2 and [Zn^{2+}-Tz] and leads to a proton transfer from [Zn^{2+}-Tz] to H_2O with the formation of H_3O^+. In fact Zn^{2+}- 1H-1,2,3-Triazole and Zn^{2+}- 2H-1,2,3-Triazole loose a proton in the presence of one water molecule, the proton migrates from the N atom of Tz to the O atom of H_2O to form hydronium ion (H_3O^+). For instance, this was observed after the addition of CO_2 around H_2O@[Zn^{2+}-1A]$_{b,S1}$, which resulted into two reactive complexes. They are denoted as S1 and S2 in Figure 6. In contrast to the weekly bonded complexes described above, the formation of

such compounds is associated with large monomer deformations upon complexation. The energies associated with these complexes are computed as 13.60 and 16.34 kcal/mol (Figure 6), i.e., much larger than the few kcal/mol described above for the non-reactive tetramer complexes formation. These strong modifications and stabilizations should influence the mutual interactions of water and CO_2 with the subunits of MOFs and of Zn-proteins (see below).

IV. Discussion

As mention in the Introduction, several molecular modeling and simulation techniques have been used to predict the structure and macromolecular properties of porous nanomaterials and metalloenzymes. In the case of water and CO_2 adsorbents present in a cavity of a porous Zn-triazole based material or in the active site of a Zn-enzyme, unsettled questions remain on how water molecule induces chemical transformation of the host sites pore surfaces to attract/repel CO_2 guest molecules, and how the removed / added moieties will chemically unconfined / confine the pores, hence altering their storage and separation capacities. In sum, we found complexes where CO_2 or water weakly binds to the organic-Zn moiety. This set of clusters is relevant to CO_2 capture and sequestration since the metal (engaged in the 3D backbone of these materials) is not expected to be in contact with CO_2 in these nanoporous materials. We also found a second class of clusters where either a covalent bond (Zn-O) is formed between Zn and O atom of CO_2 or H_2O or intramolecular proton transfer is induced upon complexations. This second class of compounds is of great importance to understand the physico- chemical processes occurring at the active sites of Zn-proteins since Zn and CO_2 and / or H_2O are mutually present there. The presence of zinc ion is thus essential for CO_2/H_2O adsorption and the stability of MOF. For instance, Boulmene et al. [56] mapped the interaction potentials between Tz and CO_2 without the presence of Zn^{2+} and they found three types of clusters which correspond to various noncovalent interactions. The most stable one is H-bond and acid–base interaction between CO_2 and the nitrogen of Tz (BE of ~ -4.5 kcal .mol^{-1}). However, in the presence of zinc ion we identified strong electron donor-acceptor complexes, in which a covalent bond between O atom of CO_2 and zinc of [Zn^{2+}-Tz] is established (BE ~ -56 kcal .mol^{-1}). Therefore, Zn ion stabilizes the complex with an intermolecular charge transfer from Zn^{2+} to Tz through the lone pair of nitrogen [40]. For macromolecular structures, the zinc should play similar role and participate to their further stabilization. The remaining unsaturated zinc sites within these Zn-containing macromolecules should enhance the interaction with adsorbents (H_2O, CO_2).

Firstly, we compare the efficiency of the bonding between CO_2 and [Zn^{2+}-Tz] and CO_2 and [Zn^{2+}-Im] complexes (Im = imidazole). [33] For the most stable complexes, the

identified type of interactions in CO_2@[Zn^{2+}-Tz] complexes is similar to that found for CO_2@[Zn^{2+}-Im] complexes. Indeed, we compute in both cases a strong covalent bond between CO_2 and Zn with similar Zn---O distances (of ~1.9 Å). Nevertheless, we compute here much more stable CO_2@[Zn^{2+}-Tz] clusters compared to CO_2@[Zn^{2+}-Im] clusters. Therefore, the well-established greater efficiency of [Zn^{2+}-Tz] subunits containing macromolecular compounds to CO_2 capture and sequestration compared to those formed by [Zn^{2+}-Im] may be related to the greater number of sites for favorable interactions within [Zn^{2+}-Tz] compared to [Zn^{2+}-Im] and to the relatively larger BEs, in absolute value, between CO_2 and [Zn^{2+}-Tz]. Indeed, the triaozole is bidentate with more unsaturated nitrogen.

Secondly, our NBO analysis reveals that there are two inter molecular charge transfers that contribute to the stability of the complexes between CO_2/H_2O and [Zn^{2+}-Tz]. Indeed, zinc centers in these systems typically act as Lewis acids that form complexes with small molecules, such as CO_2 or H_2O. The strong bonding between Zn^{2+} / N atom of triazole or Zn^{2+} / O atom of CO_2 /H_2O may be explained qualitatively by Hard Soft Acid Base (HSAB) model [57] due to the electron lone pair donation from N and O (acting like Lewis bases) to the metal ion Zn^{2+} (acting like a Lewis acid). Hard acids and bases possess large HOMO-LUMO gaps favoring ionic bonding and soft acids and bases have however small HOMO-LUMO gaps favoring covalent bonding. [58] Here, we compute rather large HOMO-LUMO gaps (e.g. E_{LUMO} - E_{HOMO} = 7.07 and 7.67 eV for CO_2@[Zn^{2+}-1B]$_{a,S3}$ and for CO_2@[Zn^{2+}-2A]$_{a,S1}$, respectively). Our microscopic first principles investigations validate the use of this simple model to explain the bonding at the interfaces of macromolecular nonporous materials and Zn-proteins with CO_2 or H_2O.

Thirdly, our computations reveal that when the metal ion Zn^{2+} is fixed on carbon atom of Tz, [Zn^{2+}-1H-1,2,3-triazole] and [Zn^{2+}-2H-1,2,3-triazole] act as Arrhenius acids. Indeed, upon addition of a water molecule, these complexes release a proton (from N---H of Tz) to form hydronium (H_3O^+). Note that we didn't observe this phenomenon in [Zn^{2+}-Tz] clusters where the zinc ion is linked to nitrogen atom of Tz, which we could explain by the large stability of these complexes compared to the ones where the zinc ion is fixed on carbon atom of Tz. So the presence of water could change the acidity of [Zn^{2+}-Tz] complexes. For instance, soft base often does not bind the proton at all in water, H_3O^+ being formed instead. [46] Moreover, the interaction between water and metal site could result in modified Bronsted acidity. [59] Indeed, the most stable type of interaction in H_2O@[Zn^{2+}-Tz], in the absence of CO_2, results from a covalent bond between O atom of H_2O and zinc atom of [Zn^{2+}- Tz] which may decrease locally their Bronsted acidity. This leads to a reduction of the binding energies between the H_2O@[Zn^{2+}-Tz] complexes and CO_2 (cf. ΔBE given in Table 2). Thus, either implicitly including the solvent effect by PCM or explicitly adding one water molecule in the

Zn^{2+}-Tz complex, point to a reduction of CO_2 uptake. On the other hand, pre-adsorbing small amount of water molecules at low pressure may enhance the capacity of the nanoporous materials (e.g. MOFs) for CO_2 uptake, since the electrostatic interactions (quadrupole moment of CO_2 and the electric field created by water molecules) may help for that purposes. Consequently, the influence of the presence of water molecule on the framework stability and CO_2 uptake depends on different parameters like pressure, quantity of added water and coordination site. Indeed the presence of cations in MOFs is expected to create a large electric field and help binding polar molecules. However the opposite effect could also be possible since the interaction between quadrupole moment of CO_2 and the electric field created by water molecules is in favor of an increase of the CO_2 uptake. [60.]

V. Conclusions

The equilibrium structures, bonding, and stability of CO_2@[Zn^{2+}-Tz] complexes in gas phase and water solution have been studied by DFT with inclusion of dispersion correction (M05-2X+D3). The most stable structures correspond to strong electron donor-acceptor complexes, in which a covalent bond between O atom of CO_2 / H_2O and Zn^{2+} of [Zn^{2+}-Tz] is established. Besides, the bonding between Tzs and CO_2 / H_2O is due to non-covalent interactions such as σ type H-bond. In addition, we identified the presence of intramolecular tautomeric equilibria converting these clusters.

Solvent effects were studied implicitly (PCM/M05-2X+D3 calculations) or explicitly via the consideration of a water molecule. The effects of the presence of one water molecule in solvent on the activation barrier of proton transfer between adjacent nitrogens of CO_2@[Zn^{2+}-Tz] are hence investigated. Results indicate that there are no significant changes in the protonation pathways during the transition from gas phase to solution, but the difference of energy between tautomers may be reduced from ~20 kcal/mol in gas phase, to ~5 kcal/mol in aqueous solution. This behavior could be explained by the correlation effects, which reduce the energy separation between the tautomers to a small extent but do not reverse the general stability. In addition, the intramolecular potential barrier of tautomerism is also deceased by ~50 kcal/mol. Thus, the tautomeric conversion is easier in water solution. By adding one H_2O molecule, we get indeed better delocalization of electronic charge, which facilitates the proton migration from N1 to N2 through the water molecule.

The findings of our theoretical study are important for understanding, at the microscopic level, of the structure and bonding within triazolate based macromolecular porous materials and Zn-enzymes. Through our study we confirmed that triazole porous materials present an exceptional capacity and selectivity for gas adsorption [61] because of the incorporation of more accessible nitrogen donor sites (compared to imidazoles), which

increases the gas uptake.

Supporting Information. Details of Natural Bond Orbital analysis and Optimized Coordinates of all identified structures are available in the Supporting Information (PDF).

Acknowledgement

S.G. acknowledges support of the Serbian Ministry of Education and Science (Grant No. 172035). We thank the COST Action CM1405 MOLecules in Motion (MOLIM) and the COST Action CA17120 Chemobrionics (CBrio) of the European Community for support.

References

1 Liu, K.; Shi, W.; Cheng, P. The Coordination Chemistry of Zn(II), Cd(II) and Hg(II) complexes with 1,2,4-triazole derivatives. *Dalton Trans.* **2011,** *40*, 8475-8490.

2 Štefane, B.; Perdih, F.; Višnjeva, A.; Požgan, F. Novel Triazole-based Ligands and their Zinc(II) and Nickel(II) Complexes with a Nitrogen Donor Environment as Potential Structural Models for Mononuclear active sites. *New J. Chem.* **2015**, *39*, 566-575.

3 Lee,H. M.; Youn, I. S.; Saleh, M.; Lee, J. W.; Kim, K. S.; Interactions of CO_2 with Various Functional Molecules, *Phys. Chem. Chem. Phys.* **2015**, *17,* 10925-10933.

4 Fleming, D. A.; Thode, C. J.; Williams, M. E. Triazole Cycloaddition as a General Route for Functionalization of Au Nanoparticles. *Chem. Mater.* **2006**, *18*, 2327-2334.

5 Li, P.Z.; Wang, X.J. ; Liu, J.; Lim, J. S.; Zou, R.; Zhao, Y. A Triazole-Containing Metal–Organic Framework as a Highly Effective and Substrate Size-Dependent Catalyst for CO_2 Conversion. *J. Am. Chem. Soc.* **2016,** *138*, 2142-2145.

6 Xie, L-H.; Suh, M. P. High CO_2-Capture Ability of a Porous Organic Polymer Bifunctionalized with Carboxy and Triazole Groups. *Chem. Eur. J.* **2013,** *19*, 11590-11597.

7 Aromí, G.; Barrios, L. A.; Roubeau, O.; Gamez, P. Triazoles and Tetrazoles: Prime Ligands to Generate Remarkable Coordination Materials. *Coord. Chem. Rev.* **2011,** *255*, 485-546.

8 Saleh, M.; Lee, H. M.; Kemp, K. C.; Kim, K. S. Highly Stable CO_2/N_2 and CO_2/CH_4 Selectivity in Hyper-cross-linked Heterocyclic Porous Polymers. *ACS Appl. Mater. Interfaces* **2014,** *6*, 7325-7333.

9 Mondal, S.; Das, N.; Triptycene based 1,2,3-triazole Linked Network Polymers (TNPs): Small Gas Storage and Selective CO_2 Sapture. *J. Mater. Chem. A* **2015,** *3*, 23577-23586.

10 Hilton, J. L.; Kearney, P.C.; Ames, B. N. Mode of Action of the Herbicide, 3-amino-1,2,4-triazole(amitrole): Inhibition of An Enzyme of Histidine Biosynthesis. *Arch. Biochem. Biophys.* **1965,** *112*, 544-547.

11 Nett, J. E.; Andes, D. R. Antifungal Agents: Spectrum of Activity, Pharmacology, and Clinical Indications. *Infect Dis. Clin. North Am.* **2016**, *30*, 51-83.

12 Holla, B. S.; Poojary, K.N.; Rao, B.S.; Shivananda, M.K. New bis-aminomercaptotriazoles and bis-triazolothiadiazoles as possible Anticancer Agents. *Eur. J. Med. Chem.* **2002** , *37*, 511– 517.

13 Ahmad, N.; Younus, H. A.; Chughtai, A. H.; Van Hecke, K.; Danish, M.; Gaoke, Z.; Verpoort, F. Development of Mixed metal Metal-organic Polyhedra Networks, Colloids, and MOFs and their Pharmacokinetic Applications. *Scientific Reports* **2017,** *7,* 832.

14 Haasnoot, J. G. Mononuclear, Oligonuclear and Polynuclear Metal Coordination Compounds with 1,2,4-triazole derivatives As Ligands. *Coord. Chem. Rev.* **2000,** *200,* 131-185.

15 Jafari, T.; Moharreri,V.; Toloueinia, P.; Shirazi Amin, A.; Sahoo, S.; Khakpash, N.; Noshadi, I.; Alpay, S. P.; Suib, S. L.; Microwave-assisted Synthesis of Amine Functionalized Mesoporous Polydivinyl benzene for CO_2 Adsorption. *Journal of CO_2 Utilization* **2017,** *19*, 79-90.

16 Liu, J. J.; He, X.; Shao, M.; Li, M. X. Syntheses, Structures and Thermal Stabilities of Four Complexes with 4-amino-3,5-bis(3-pyridyl)-1,2,4-triazole Ligand. *J. Mol. Struct.* **2008,** *891,* 50-57.

17 Hong, M. Inorganic−Organic Hybrid Coordination Polymers: A New Frontier for Materials Research. *Cryst. Growth Des.* **2007,** *7,* 10-14.

18 Li, H.; Zheng, Q.; Han, C. Click Synthesis of Podand Triazole-linked Gold Nanoparticles as Highly Selective and Sensitive Colorimetric Probes for lead(II) ions. Analyst, RSC **2010,** *135*, 1360-1364.

19 Wang, X.-J.; Li, P.-Z.; Chen, Y.; Zhang, Q.; Zhang, H.; Chan, X. X.; Ganguly, R.; Li, Y.; Jiang, J.; Zhao, Y.; Metal-Organic Framework and Its Exceptionally High CO_2 and

H_2 Uptake Capability. *Scientific Reports* **2013,** *3*, 1149.
20 Boussouf, K. ; Khairat, T.; Prakash, M.; Komiha, N.; Chambaud, G.; Hochlaf, M.; Structure, Spectroscopy, and Bonding within the Zn^{q+}–$Imidazole_n$ (q = 0, 1, 2; n = 1–4) Clusters and Implications for Zeolitic Imidazolate Frameworks and Zn–Enzymes. *J. Phys. Chem. A* **2015,** *119*, 11928-11940.
21 Linder, D. P.; Rodgers, K. R.; Methanethiol Binding Strengths and Deprotonation Energies in Zn(II)-Imidazole Complexes from M05-2X and MP2 Theories: Coordination Number and Geometry Influences Relevant to Zinc Enzymes. *J. Phys. Chem. B* **2015,** *119*, 12182-92.

22 Vaidhyanathan , R.; Iremonger, S. S.; Dawson, K. W. ; Shimizu, G. K. H. An amine-functionalized Metal Organic Framework for Preferential CO_2 Adsorption at Low Pressures. *Chem. Commun.* **2009,** *35*, 5230-5232.

23 Demessence, A.; D'Alessandro, D. M.; Lin Foo, M.; Long, J. R. Strong CO_2 Binding in a Water-Stable, Triazolate-Bridged Metal−Organic Framework Functionalized with Ethylenediamine. *J. Am. Chem. Soc.* **2009,** *131,* 8784-8786.
24 Hussain, M. A.; Soujanya, Y.; Sastry, G. N. Computational Design of Functionalized Imidazolate Linkers of Zeolitic Imidazolate Frameworks for Enhanced CO_2 Adsorption. *J. Phys. Chem. C* **2015,** *119,* 23607-23618.
25 Vogiatzis, K. D.; Mavrandonakis, A.; Klopper, W.; Froudakis, G. E.; Ab initio Study of the Interactions between CO_2 and N-containing Organic Heterocycles. *Chem.Phys.Chem* **2009,** *10,* 374-383.
26 Joos, L.; Swisher, J. A.; Smit, B.; Molecular Simulation Study of the Competitive Adsorption of H_2O and CO_2 in Zeolite 13X. *Langmuir*, **2013,** *29* , 15936-15942.
27 Li, G.; Xiao, P.; Webley, P. A.; Zhang, J.; Singh, R. Competition of CO_2/H_2O in Adsorption based CO_2 Capture. *Energy Procedia* **2009,** *1*, 1123-1130.
28 Li, G.; Xiao, P.; Webley, P.; Zhang, J.; Singh, R.; Marshall, M.; Capture of CO_2 From High Humidity Flue Gas by Vacuum Swing Adsorption with Zeolite 13X. *Adsorption* **2008,** *14***,** 415-422.
29 Yazaydın, A. O.; Benin, A. I.; Faheem, S. A.; Jakubczak, P.; Low, J. J.; Willis, R. R.; Snurr, R. Q. ; Enhanced CO_2 Adsorption in Metal-Organic Frameworks via Occupation of Open-Metal Sites by Coordinated Water Molecules. *Chem. Mater.* **2009,** *21,* 1425-1430.
30 Soubeyrand-Lenoir, E.; Vagner, C.; Yoon, J. W.; Bazin, P.; Ragon, F.; Hwang, Y. K.; Serre, C.; Chang, J.-S.; Liewellyn, P. L. How Water Fosters a Remarkable 5-fold Increase in Low-Pressure CO_2 uptake within Mesoporous MIL-100(Fe). *J. Am. Chem. Soc*. **2012,** *134*, 10174-10181.
31 Trickett, C. A.; Osborn Popp, T. M. ; Su, J. ; Yan, C.; Weisberg, J.; Huq, A.; Urban, P. ; Jiang, J. ; Kalmutzki, M. J.; Liu, Q.; Baek, J.; Head-Gordon, M. P. ; Somorjai, G. A.; Reimer, J. A. ; Yaghi, O. M. Identification of the Strong Brønsted Acid site in a Metal-organic Framework Solid Acid Catalyst. *Nature chemistry*, **2019,** *11*, 170-176.
32 Burtch, N. C.; Jasuja, H.; Walton, K. S. Water Stability and Adsorption in Metal-organic Frameworks. *Chem. Rev.* **2014,** *114,* 10575-10612.
33 Boulmene, R.; Boussouf, K.; Prakash, M.; Komiha, N.; Al-Mogren, M. M.; Hochlaf, M. Ab Initio and DFT Studies on CO_2 Interacting with $Zn(^{q+})$-Imidazole (q=0, 1, 2) Complexes: Prediction of Charge Transfer through σ- or π-Type Models. *Chem.Phys.Chem.* **2016,** *17,* 994 -1005.
34 Prakash, M.; Mathivon, K.; Benoit, D. M.; Chambaud, G.; Hochlaf, M. Carbon dioxide Interaction with Isolated Imidazole or Attached on Gold Clusters and Surface: Competition between σ H-bond and π stacking Interaction. *Phys. Chem. Chem. Phys.* **2014,** *16,* 12503-12509.
35 Linder, D. P.; Baker, B. E.; Rodgers, K. R. $[(H_2O)Zn(Imidazole)_n]^{2+}$: The Vital

Roles of Coordination Number and Geometry in Zn-OH_2 Acidity and Catalytic Hydrolysis. *Phys. Chem. Chem. Phys.* **2018,** *20,* 24979-24991.
36 Grauffel, C.; Lim, C. Factors Governing when a Metal-bound Water is Deprotonated in Proteins. *Phys. Chem. Chem. Phys.* **2018,** *47*, 29625 -29636.
37 Parkin, G. Synthetic Analogues Relevant to the Structure and Function of Zinc Enzymes*, Chem. Rev*. **2004,** *104*, 699-767.
38 Duncan, M.A.; Advances in Metal and Semiconductor Clusters: Metal Ion Solvation and Metal-Ligand Interactions ; Elsevier Science, 2001.
39 Peschke, M.; Blades, A. T.; Kebarle, P. Metalloion−Ligand Binding Energies and Biological Function of Metalloenzymes Such as Carbonic Anhydrase. A Study Based on ab Initio Calculations and Experimental Ion−Ligand Equilibria in the Gas Phase. *J. Am. Chem. Soc.* **2000,** *122*, 1492-1505.
40 Dahmani, R.; Ben Yaghlane, S.; Boughdiri, S.; Mogren Al-Mogren, M.; Prakash, M.; Hochlaf, M. Insights on The Interaction of Zn2+ cation with Triazoles: Structures, Bonding, Electronic Excitation and Applications. *Spectrochim Acta A Mol Biomol Spectrosc.* **2018,** 193, 375-384.
41 Sorkin, A.; Truhlar, D. G.; Amin, E. A. Energies, Geometries, and Charge Distributions of Zn Molecules, Clusters, and Biocenters from Coupled Cluster, Density Functional, and Neglect of Diatomic Differential Overlap Models. *J. Chem. Theory Comput.* **2009,** *5,* 1254-1265.
42 Amin, E. A.; Truhlar, D. G. Zn Coordination Chemistry: Development of Benchmark Suites for Geometries, Dipole Moments, and Bond Dissociation Energies and Their Use To Test and Validate Density Functionals and Molecular Orbital Theory. *J. Chem. Theory Comput.* **2008,** *4*, 75-85.
43 Zhao, Y.; Schultz, N. E.; Truhlar D. G. Design of Density Functionals by Combining the Method of Constraint Satisfaction with Parametrization for Thermochemistry, Thermochemical Kinetics, and Noncovalent Interactions. *J. Chem. Theory Comput.* **2006,** *2,* 364-382.
44 Boussouf, K.; Boulmene, R.; Prakash , M.; Komiha, N.; Taleb, M.; Al-Mogren, M.M.; Hochlaf, M. Characterization of Zn^{q+}–imidazole (q= 0, 1, 2) Organometallic Complexes: DFT Methods vs. Standard and Explicitly Correlated post-Hartree–Fock Methods. *Phys. Chem. Chem. Phys.*, **2015,** *17,* 14417-14426.
45 Grimme, S.; Antony, J.; Ehrlich, S.; Krieg, H. A consistent and Accurate Ab initio Parametrization of Density Functional Dispersion Correction (DFT-D) for the 94 elements H-Pu. *J. Chem. Phys.*, **2010,** *132,* 154-104.
46 Frisch, M. J.; Trucks G. W.; Schlegel, H. B.; Scuseria, G. E. ; Robb, M. A. ; Cheeseman, J. R. ; Scalmani, G.; Barone, V.; Mennucci, B.; Petersson, G. A. GAUSSIAN 09, Revision D.01, Gaussian, Inc., Wallingford CT, **2013**.
47 Tomasi, J.; Persico, M. Molecular Interactions in Solution: An Overview of Methods Based on Continuous Distributions of the Solvent. *Chem. Rev.* **1994**, *94*, 2027-2094.
48 Cramer, C. J.; Truhlar, D.G.; Implicit Solvation Models: Equilibria, Structure, Spectra, and Dynamics, *Chem. Rev.* **1999**, *99*, 2161-2200.
49 Gonzalez, C.; Schlegel ,C. An improved Algorithm for Reaction path Following. *J. Chem. Phys.* **1989**, *90,* 2154-2161.
50 Gonzalez, C. ; Schlegel, H. B. Reaction Path Following in Mass-weighted Internal Coordinates. *J. Phys. Chem.* **1990,** *94*, 5523-5527.
51 NBO 6.0. Glendening, E. D.; Badenhoop, J.K.; Reed, A. E.; Carpenter, J. A. Bohmann, C. M. Morales, Landis, C. R.; Weinhold, F. Theoretical Chemistry Institute, University of Wisconsin, Madison **(2013)**.
52 Boys, S. F.; Bernardi,F. The calculation of Small Molecular Interactions by The Differences of Separate Total Energies. Some Procedures with Reduced Errors. *Mol. Phys.* **1970,** *19,* 553-566.
53 Cox, J. R.; Woodcock , S.; Hillier, I. H.; Vincent , M. A. Tautomerism of 1,2,3-

and 1,2,4-triazole in the Gas Phase and in Aqueous Solution: A Combined Ab initio Quantum Mechanics and Free Energy Perturbation Study. *J. Phys. Chem.* **1990,** *94,* 5499-5501.

54 Subbaraman, R.; Ghassemi, H.; Zawodzinski Jr, T. Triazole and Triazole Derivatives As Proton Transport Facilitators in Polymer Electrolyte Membrane Fuel Cells. *Solid State Ionics* **2009**, *180,* 1143-1150.

55 Oziminski, W. P. The Kinetics of Water-assisted Tautomeric 1,2-proton Transfer In Azoles: A Computational Approach. *Struct. Chem.* **2016,** ***27,*** 1845-1854.

56 Boulmene, R.; Prakash, M.; Hochlaf M. Microscopic investigations of site and functional selectivity of triazole for CO_2 capture and catalytic applications. *Phys. Chem. Chem. Phys.* **2016**,*18*, 29709-29720 .

57 Pearson, R. G. Hard and Soft Acids and Bases. *J. Am. Chem. Soc.* **1963,** *85*, 3533-3539.

58 Trojer , M. A.; Movahedi A.; Blanck, H.; Nydén M. Imidazole and Triazole Coordination Chemistry for Antifouling Coatings. *Journal of Chemistry* **2013,** *23*, 946739.

59 Jiang, J.; Yaghi, O. M. Brønsted Acidity in Metal–Organic Frameworks.*Chem. Rev.* **2015,** *115*, 6966−6997.

60 Yazaydın, A. O.; Benin, A. I.; Faheem, S. A.; Jakubczak, P. ; Low, J. J.; Willis, R. R.; Snurr, R. Q. Enhanced CO 2 Adsorption in Metal-Organic Frameworks via Occupation of Open-Metal Sites by Coordinated Water Molecules. *Chem. Mater.* **2009**, *21*, 1425–1430.

61 Suh, M. P. Metal-Organic Frameworks and Porous Coordination Polymers: Properties and Applications, *Bull. Jpn. Soc. Coord.Chem.*, **2015,** *65,* 9-22.

TOC Graphic